Nuclear Instruments and Methods in Physics Research B 548 (2024) 165249

Contents lists available at ScienceDirect

Nuclear Inst. and Methods in Physics Research, B

journal homepage: www.elsevier.com/locate/nimb

# The SPES laser ion source: Time structure, laser enhancement and efficiency measurements with gallium at ISOLDE Offline 2

O.S. Khwairakpam [a,b,*], R. Mancheva [c,d], M. Au [c], C. Bernerd [c,d], L. Centofante [b], K. Chrysalidis [c], B. Crepieux [c], V.N. Fedosseev [c], R. Heinke [c], T. Marchi [b], E. Mariotti [a,e], B.A. Marsh [c], A. Monetti [b], P. Nicolosi [f], S. Rothe [c], D. Scarpa [b], M. Schuett [c], T. Stora [c], A. Andrighetto [b], M. Manzolaro [b]

[a] DSFTA, University of Siena, Via Roma 56, Siena, 53100, Italy
[b] INFN-LNL, Viale Università 2, Legnaro, Padova, 35020, Italy
[c] CERN SY-STI, Espl. des Particules 1, Geneva, 1211, Switzerland
[d] KU Leuven, Instituut voor Kern- en Stralingsfysica, Leuven, 3001, Belgium
[e] INFN, Sezione di Pisa, Largo Bruno Pontecorvo, 3/Edificio C, Pisa, 56127, Italy
[f] CNR IFN, University of Padova, Via Trasea 7, Padova, 35131, Italy

ARTICLE INFO

*Keywords:*
Laser ion source
Hot cavity
Time structure
Laser enhancement
Radioactive ion beams
SPES
ISOLDE

ABSTRACT

The SPES laser ion source has been tested at ISOLDE Offline 2, CERN. A two-step single resonance photo-ionization scheme has been used to ionize gallium atoms in the SPES tantalum hot-cavity ion source. The ion beam time structure, laser enhancement of ion yield, and ionization efficiency are investigated in relation to the ion source temperature and ion load. From the time structures, it is inferred that a significant fraction of the extracted ions are generated in the transfer line rather than just in the hot cavity. The effect of the electrostatic axial field on the movement of ions inside the ion source is discussed. Generally, there is an inverse relationship between total ion load and the laser enhancement factor. This dependency is enhanced at lower operating temperature of the ion source. This is explained by the influence of thermionic electron emission and ion density on the transverse laser-ion confinement, and therefore the survival of ions as they drift towards the extraction region of the ion source. At 2200 °C, the nominal temperature for on-line operation of the ion source, the ratio of laser-ionized to surface-ionized gallium was stable around 55 during the measurement campaign, and independent of the total extracted ion current up to the measured value of 1.1 μA. A resonance laser ionization efficiency value of 27.2% for gallium has been measured.

## 1. Introduction

The availability of radioactive ion beams (RIBs) offers unique and exciting opportunities to study the structure of nuclei far from stability and paves the way to deeper understanding of the stellar processes which govern the universe. Many leading RIB facilities are working towards developing the most versatile and efficient methods of radioactive ion production utilizing the isotope separation on-line (ISOL) technique [1,2].

At Legnaro National Laboratories (LNL), a second-generation ISOL facility named "Selective Production of Exotic Species" (SPES) is in the final stage of construction [3,4]. In the SPES project, a multi-foil target system of uranium carbide will be used [5]. When this target is irradiated by a proton beam with an energy of 40 MeV and a current intensity up to 200 μA, a fission rate of approximately $10^{13}$ $s^{-1}$ is expected inside the target. The fission fragments will effuse through a heated transfer line to the ion source, where they can be ionized and extracted for subsequent delivery to the experimental areas.

The target system can be coupled to different types of ion sources tailored to the production of specific ion beams. In this article, the extensive study and characterization of the SPES laser ion source is reported, in relation to the production of a gallium beam, which is one of the first elements that will be delivered by the SPES facility.

## 2. Resonance photo-ionization and SPES laser ion source

One of the fundamental requirements for the study of radioisotopes at ISOL facilities is the possibility of producing isotopically clean ion beams with minimal isobaric interference. The laser ion source is commonly the preferred choice, since it offers the best elemental selectivity, which neither the surface nor the plasma ion sources can deliver [6].

* Corresponding author at: DSFTA, University of Siena, Via Roma 56, Siena, 53100, Italy.
*E-mail address:* omorji.khwairakpam@student.unisi.it (O.S. Khwairakpam).

https://doi.org/10.1016/j.nimb.2024.165249
Received 21 July 2023; Received in revised form 24 December 2023; Accepted 11 January 2024
Available online 18 January 2024

For many elements, it is also the most efficient ionization method at on-line isotope separators and RIB facilities such as ISOLDE [7] or TRIUMF [8]. The step-wise photo-ionization method [9,10] serves as the foundation for the resonance ionization laser ion source (RILIS). It exploits the unique electronic energy level structures of the elements, where it selectively promotes an electron beyond the ionization potential.

The wavelength-tunable lasers allow us to precisely match the frequency of the photons to the transition energy of the valence electron(s) of a particular element. When the photons are guided into a vapor of several elements, they will exclusively excite the electrons of the atoms of the targeted element. The valence electron is successively promoted by laser photons through the energy level structure of the atom leading finally to either high-lying Rydberg states below the ionization potential (IP), auto-ionizing states or directly into the continuum through the so-called non-resonant excitation.

### 2.1. Hot cavity RILIS

A very efficient and widely implemented use of laser ion source is a hot cavity RILIS, pioneered at PNPI Gatchina and CERN [11,12]. This type of ion sources is particularly attractive because it combines the intrinsic elemental selectivity of resonance laser ionization, high ion production efficiency (typically >10%), as well as robustness of construction required for production of radioactive ion beams at ISOL facilities [7,12–15].

In this technique, typically, pulsed laser beams are overlapped in time and in space along the axis of the hot cavity of a tubular surface ion source. A confining plasma is formed in the hot cavity as a result of the presence of ionized atoms and the thermionically emitted electrons from the heated walls. This plasma has a negative potential with respect to the wall of the cavity and thus confines the ions inside the volume of the hot cavity [16,17].

In a hot cavity, ions are also created due to surface ionization from the hot wall of the cavity itself. For a single atom-wall interaction, the Saha-Langmuir equation [18] can be used to describe the relative proportion of the ionic density $n_i$ to the atomic one $n_o$ in thermal equilibrium. This is also termed as the degree of surface ionization $\alpha$,

$$\alpha = \frac{n_i}{n_o} = \frac{g_i}{g_o} exp\left(\frac{\phi - W_i}{k_B T}\right) \tag{1}$$

where $\phi$ is the work function of the cavity material, $W_i$ is the ionization energy of the element of interest, $g_i$, and $g_o$ are the statistical weights of the ionic and atomic ground states, $k_B$ is the Boltzmann constant and $T$ is the absolute temperature.

When the excitation level of the element (atom) or its ion is comparable with the thermal energy $k_B T$, the ratio of the statistical weights $g_i/g_o$ in the above expression is replaced by the ratio of the partition functions $Q_i/Q_o$ [19,20]:

$$Q_x = g_x + \sum_j g_{jx} exp(-E_{jx}/k_B T) \tag{2}$$

where $E_j$ is the excitation energy of a particular state of the atom $(x = o)$ or the ion $(x = i)$.

In such a case, the degree of ionization $\alpha$ can be expressed as

$$\alpha = \frac{Q_i}{Q_o} exp\left(\frac{\phi - W_i}{k_B T}\right) \tag{3}$$

The surface ionization efficiency $\beta$ can be expressed in terms of $\alpha$ with a simple relation given by,

$$\beta = \frac{n_i}{n_i + n_o} = \frac{\alpha}{1 + \alpha} \tag{4}$$

However, in a hot cavity the observed surface ionization efficiency is much higher than the values calculated using Eqs. (1) and (4). This is due to the multiple atom-wall collisions in the hot cavity which provides a larger chance for the atoms to be ionized. Once the ions are formed, they are trapped by the confining plasma and therefore protected until the point of extraction. This is an effect of the hot cavity. This enhancement in the ionization efficiency value is interpreted in terms of an amplification factor $N$ [17], which in turn consists of the mean number of wall collisions, and effective ion survival factor. Therefore, for a hot cavity the effective ionization efficiency value can be calculated as,

$$\alpha_c = \alpha \cdot N \tag{5}$$

$$\beta_c = \frac{\alpha_c}{1 + \alpha_c} = \frac{\alpha \cdot N}{1 + \alpha \cdot N} = \frac{\beta \cdot N}{1 - \beta(1 - N)} \tag{6}$$

The electron density $n_{es}$ along the walls, which induces the negative potential for ion confinement in the volume of the cavity, is expressed by the Richardson equation:

$$n_{es} = 2\left(\frac{2\pi m k_B T}{h^2}\right)^{3/2} exp\left(\frac{-\phi}{k_B T}\right) \tag{7}$$

From Eqs. (1), (5), (6) and (7), it can be clearly deduced that a cavity material of lower work function $\phi$ will provide lower surface ionization and, at the same time, a better ion confinement at a given temperature compared to materials of higher $\phi$ due to the increased thermionic emission of electrons. Materials of lower work function are, hence, favorable for higher performance of hot cavity RILIS [21], provided sufficient robustness at desired operation temperatures.

The SPES laser ion source is made of tantalum which has a lower work function value of 4.28 eV, compared to other materials such as tungsten (4.54 eV) and rhenium (4.96 eV), which can also operate at high temperatures above 2000 K and are typically used for surface ion sources. The work function values are taken from [22].

As mentioned earlier, the reported study is based on the production of gallium ions in the SPES laser ion source. It is, therefore, important also to understand the contribution of the surface ionization in the overall production. Eqs. (2)–(4) are used to evaluate the expected surface ionization efficiency of gallium in a tantalum cavity operating at 2200 °C, described in Section 4.4.

### 2.2. SPES Laser Ion Source (SPES-LIS)

As with most hot cavity laser ion sources, the SPES-LIS also works by introducing frequency-tuned laser beams into the volume of the surface ion source from the ion extraction side. The SPES-LIS is based on the SPES surface ion source reported in [23], which utilizes the identical mechanical structure of the ion source to produce surface ions of several elements. The geometry of the ion source has been realized as a result of the thermal optimization of the ISOLDE MK1 ion source [24], to reduce cold spots in the transfer line and higher temperature uniformity over the entire length of the ion source.

The SPES-LIS is composed of a hot cavity, a transfer line and, an alignment system. The hot cavity is a 33 mm long tubular cavity made of tantalum, with an internal diameter of 3.1 mm and an external diameter of 5.1 mm. The hot cavity is connected to the transfer line, whose other end is connected to the production target. The transfer line is a tantalum tube, approximately 70 mm long, and has an internal diameter and external diameter of 8 mm and 8.8 mm, respectively. For this offline test, no target container was present and the atom samples were introduced at the beginning of the transfer line via two independent resistively heated tantalum capillaries.

An important feature of the SPES-LIS is the “hot-cavity alignment system”. It is a circular graphite frame around the junction point of the ion source and the transfer line. It has four centering pins, made of tungsten, ensuring an axial alignment of the hot cavity as shown in Fig. 1.

This alignment system helps in mitigating the effects of thermal expansion. Having the hot cavity and the transfer line aligned in this way is expected to positively influence the laser ion production by

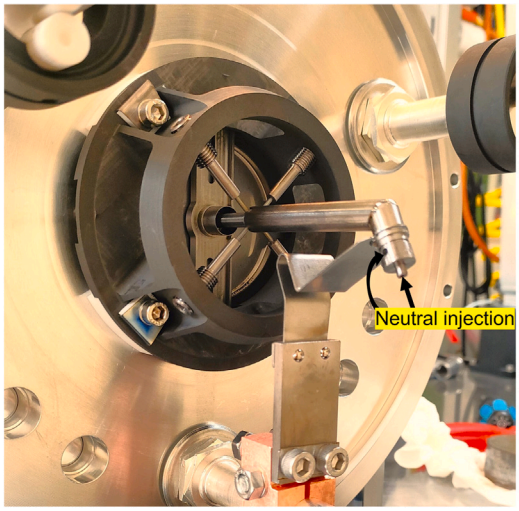


**Fig. 1.** The SPES laser ion source: the hot cavity, the transfer line, and the hot-cavity alignment system.

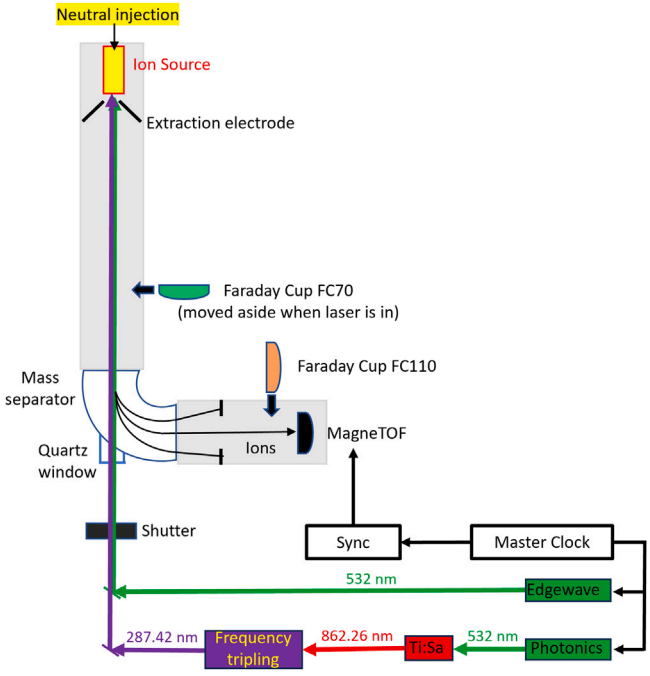


**Fig. 2.** Schematic representation of the laser system, the laser ion source and the mass-separator, and the MagneTOF™ detector used for time-structure measurement. For laser enhancement and ionization efficiency measurements, a Faraday cup is used in place of the MagneTOF™.

maintaining a mechanically stable laser-atom-interaction volume. In the absence of such a system, the interaction volume could be reduced if there is tilting of the ion source or the transfer line due to thermal deformation.

## 3. Experimental set-up

The characterization of the SPES laser ion source was performed in CERN. The ion source, composed of the hot cavity, the alignment system and, the transfer line, was installed at the ISOLDE Offline 2 facility [25–27]. The hot cavity laser ion source was mounted on the high-voltage platform at a potential of 30 kV. The collimated laser beams entered the beamline under vacuum through a quartz window in the vacuum chamber of the mass-separator dipole magnet. An electrically controlled shutter is placed in front of the window to facilitate blocking and unblocking of the laser beams during the experiment. A simplified schematic representation of the experiment is shown in Fig. 2.

The laser beams were focused through the extraction electrode orifice into the ion source. The ions generated in the ion source are extracted anti-collinearly with respect to the laser beam. The singly charged ions are accelerated to 30 keV via the extraction electrode and directed into a 90 degree field sector dipole magnet. The isotope-purified beam after the magnet is directed either to a MagneTOF™ detector [28] or a Faraday Cup FC110, depending on the measurement which is being conducted.

An additional Faraday Cup FC70 is available before the mass separator magnet, in order to read the total ion current from the ion source in the "laser off" condition.

### 3.1. Modes of measurements

In order to characterize the laser ion source, three different kinds of measurements were performed: ion beam time structure, laser enhancement of ion yield, and ionization efficiency.

*Time structure profiles*

The lasers utilized for resonance ionization are typically pulsed at repetition rates of 10 kHz, with pulse lengths ranging from a few ns to tens of ns. This rate ensures that each atom interacts with at least one laser pulse during the time it resides inside the cavity. It is considered to be a good compromise between achieving enough pulse energy to saturate atomic transitions and number of laser-atom interactions for a typically achievable value of average power. The simultaneous creation of ions all along the ion source volume by a laser pulse leads to a periodic modulation of the extracted ion beam, governed by the source-internal extraction mechanisms. Therefore, the resulting time structure of the ion beam can give information about the ion source environment. This technique has been well-described in other previous works [12,21,29,30].

To obtain such time structures, a MagneTOF™ detector in single ion counting mode is used to investigate the isotope beam after mass separation. The readout is synchronized with the trigger of the laser pulses. The single ion counts on the detector were used to create a histogram of ion arrival times with respect to the trigger of the laser pulses, as registered by a Cronologic TimeTagger4 acquisition module, described in [26]. To avoid time-overlap of the extracted bunches, a laser repetition rate of 5 kHz was employed, thus the temporal window for each profile is 200 μs. Multiple hundred thousands of laser pulses and the produced ions are registered to obtain an averaged time structure for each operational setting of the ion source.

*Laser enhancement ratios*

For a hot cavity laser ion source, the production of ions through surface ionization is unavoidable. The ratio of the ions produced by the laser interaction (laser ions) compared to the ones produced by the surface ionization (surface ions) determines the selectivity of the laser ion source.

During these measurements, the isotope-specific (mass-separated) ion current value is recorded with the ionizing laser beams sent in-to the ion source cavity and repeated after blocking the lasers. The ratio of the former to the latter gives the laser enhancement ratio (LER). For these measurements, a Faraday Cup is introduced just in front of the MagneTOF™ detector to read the instantaneous isotopic ion current.

*Ionization efficiency*

The measurements of surface ionization efficiency and laser ionization efficiency were performed using the procedure described in the following sections. A calibrated sample of a precisely known quantity of atoms is used to inject the atoms gradually into the ion source, while the ionization process is running and produced ion current is continuously measured until the total exhaustion of the sample. At the end of the measurement, the total number of detected ions is deduced from time-integration of the ion current measurements. The ratio of this number to the initial number of atoms in the sample gives the ionization efficiency value.

It is important to note that, for laser ion sources, the efficiency depends on a variety of factors: sample volatilization and atomization, the employed ionization scheme, the extraction, transport and detection efficiency. All of these factors can independently change, giving rise to overall efficiency differences when employing the same laser ionization scheme at different mass separator facilities.

### 3.2. Sample preparation

The samples were introduced into capillaries made from tantalum. By attaching these capillaries to the back of the transfer line and gradually heating them, a supply of neutrals into the ion source is ensured [31].

Gallium (Ga) has two stable isotopes: $^{69}$Ga and $^{71}$Ga with natural abundances of 60.11% and 39.89%, respectively. A solution of gallium in 5% $HNO_3$/tr. HCl, of known concentration (1 μg of Ga/μL), was used to produce the Ga sample used for the measurement. Assuming 100% conversion to singly-charged ions, 1 μg of Ga atoms would correspond to the total charge of 380 nAh in both isotopes. The original solution of 1 μg of Ga/μL was diluted 100 times giving a new concentration of 0.01 μg of Ga/μL. A single drop (of 10 μL) would now contain 38 nAh of Ga. For efficiency tests, gallium samples of 76 nAh and 114 nAh were used, which correspond to 20 μL and 30 μL, respectively, of the final diluted solution.

Drops of the solution were put on a small piece of tantalum foil and left to dry. Once the solution was dried completely, the foil was folded and inserted into the narrow capillary of the sample reservoir. After the sample was inserted (just a few mm into the capillary), the capillary was tightly squeezed on one end and the other end was connected to the transfer line. Gradual heating of the tantalum capillary leads to evaporation of the gallium sample and release of the gallium atoms into the ion source via effusion. The flux of atoms was regulated by the heating current using a dedicated power supply.

For the laser enhancement and time structure measurements, excess gallium samples (roughly 7600 nAh) were used. In this case, around 20 μL of the original concentration of the solution was used.

It is essential to understand how the laser ion confinement and the selectivity are affected by the presence of other ions (impurities) [16,17]. For this purpose, an additional sample of barium (Ba) was attached to the transfer line. As barium is efficiently surface-ionized at high temperatures, it can be used to independently manipulate the ion load in the ion source.

### 3.3. Photo-ionization scheme of gallium and the laser system

The photo-ionization scheme used during this experiment to laser ionize the gallium atoms [32] is shown in Fig. 3.

To produce the wavelengths required for the indicated scheme, a titanium:sapphire (Ti:Sa) laser [33] was used and the generated fundamental light was subsequently frequency tripled to 287.422 nm. For non-resonant excitation into the continuum, a single mode frequency-doubled Edgewave PX200-2-GF-SLM laser (for the 532 nm) was used.

The Ti:Sa laser was pumped with a frequency-doubled Nd:YAG laser Photonics DM60 operated at a power of 11–11.5 W. A HighFinesse/Angstrom WS6-600 wavelength meter was used to continuously

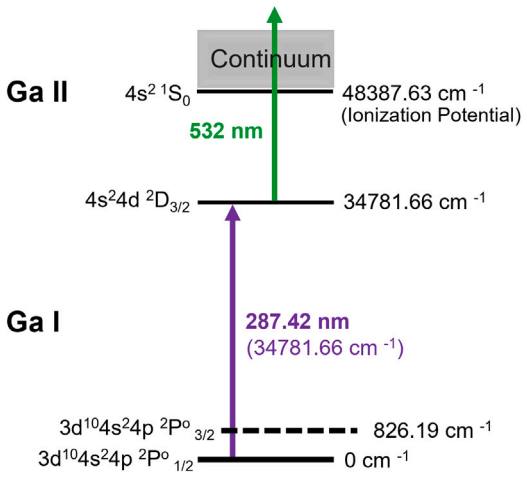


**Fig. 3.** Photo-ionization scheme of gallium used for ionization from the atomic ground state. The dotted line indicates the first thermally excited state. The wavelengths indicated are in air.

monitor the fundamental wavelength of the output of the Ti:Sa laser. The Ti:Sa laser was tuned to produce a fundamental IR laser output at 11 593.89 $cm^{-1}$ (862.264 nm). The output fundamental beam was sent to the frequency tripling unit where the desired, resonant laser beam at 34 781.66 $cm^{-1}$ (287.422 nm) was generated. After passing through a telescope which comprises a combination of cylindrical and spherical lenses, the beam was sent to the ion source. The power of the UV beam was maintained at around 100 mW before the vacuum entrance window of the mass separator, which is sufficient for the saturation of the electronic transition.

The power of the green beam applied for the non-resonant step was around 20 W at the vacuum entrance window, except during the time structure measurement where power was reduced to limit the number of ions produced to stay within safe operation regime of the detector. The green laser beam was sent to the ion source after passing through a telescope of spherical lenses. The delay of the green laser pulses with respect to the UV laser pulses was electronically adjustable and optimized according to the ion-current readout.

## 4. Measurement sessions and results

### 4.1. Thermal-electrical characterization

Before the SPES ion source system was mounted on the front-end high-voltage platform, calibration of the ion source temperature with respect to the heating current was performed. The ion source heating was obtained by applying a DC current from the beginning of the transfer line (where neutrals are injected, see Fig. 1) up to the exit of the hot cavity.

Fig. 4 shows the various calibration cycles performed and the temperature reading from an inner point of the ion source against the heating current. A filament pyrometer, aligned close to the mid-point of the hot cavity, was used to take the temperature readings. The ion source showed a very reproducible thermal behavior during the heating and cooling cycles of the measurement.

For the same cycles of thermal calibration performed, the electric potential difference values detected at the power supply were also noted, shown in Fig. 5. In the conventional use of the ion sources, the polarity is applied in such a way that the beginning of the transfer line is maintained at a higher voltage potential and it gradually drops towards the exit of the hot cavity. This provides an axial field that favors the drifting of the ions, inside the ion source, towards the exit for extraction [12,29,30,34].

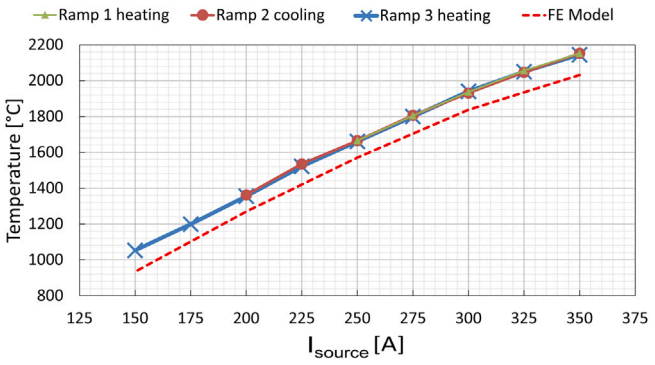


**Fig. 4.** Experimental temperatures close to the mid-point of the hot-cavity and comparison to the Finite Element (FE) Model results, at different applied heating current.

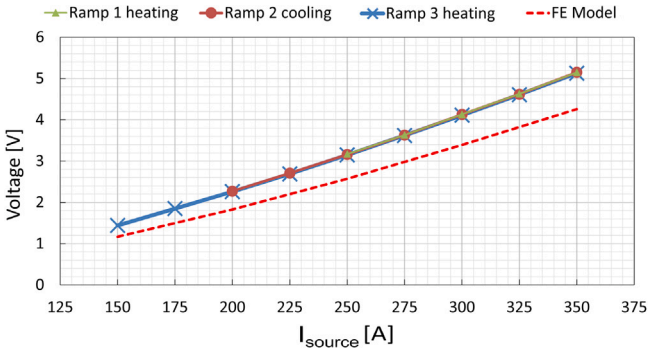


**Fig. 5.** The electric potential difference values detected at the power supply and comparison to the Finite Element (FE) Model results, at different applied heating current.

Both in Figs. 4 and 5, the measured values are higher than the values obtained from the Finite Element (FE) Model, developed and presented in [23]. This is explained by the fact that in the FE model, the simulations were performed considering an ideal contact between the surfaces. The temperature distribution and the potential gradient along the whole length of the transfer line and the hot cavity for the SPES ion source at different heating currents have been studied before and can be found in [23].

### 4.2. Time structure of gallium ions

For ion beam time structure measurements, the separation magnet was tuned to the gallium isotope of mass 71 u. As described in Section 3.1, the ion beam of $^{71}Ga^{+}$ was directed onto a MagneTOF™ detector. The average ion current was kept below 500 fA (corresponding to around 300,000 ions per second) as the detector was used in single ion counting mode. The power of the green laser beam was reduced to around 10–20 mW, just enough to produce laser ions whilst staying below the safety limit of the operation mode of the detector.

The time structure measurements were performed for different ion source temperatures at 2200 °C, 2050 °C, 1940 °C, and 1800 °C. The time structure of the laser ions (after subtracting the surface ions) at different temperatures are shown in Fig. 6. In all the time profiles, t = 0 is given by the trigger of the laser pulse. Three main peaks are observed: first around 18 μs, second between 45–55 μs, and third between 70–85 μs.

The first peak is the pre-bunch of ions that are formed in the outermost part of the ion source, and extracted almost immediately by the penetrating extraction field. This region is indicated as "1" in Fig. 7 and typically extends inwards by exactly the same value as the opening diameter of the ion source. This "fast extraction" peak was also observed and discussed in several RILIS studies [29,30].

The second bunch originates from the hot cavity of the ion source, indicated as region 2 in Fig. 7. The third bunch is from the transfer line (region 3) connecting the hot cavity to the atom source (sample holder capillary in this particular case). It is clear that a large proportion of the extracted ions originates from the transfer line. This means the confining plasma is present not only in the hot cavity but also in the transfer line, as was also found for a similar ion source presented in [30]. This is a consequence also of the presence of the axial potential gradient in the transfer line. The third bunch is not observed in systems where the ion guide is limited to the hot cavity, for example in the ISOLDE RILIS cavity [12,29] where the transfer line is passively heated.

### *Axial electric field and movement of the ions*

Looking at the profiles at different temperatures, it can be clearly observed that apart from the first pre-bunch, all the other bunches

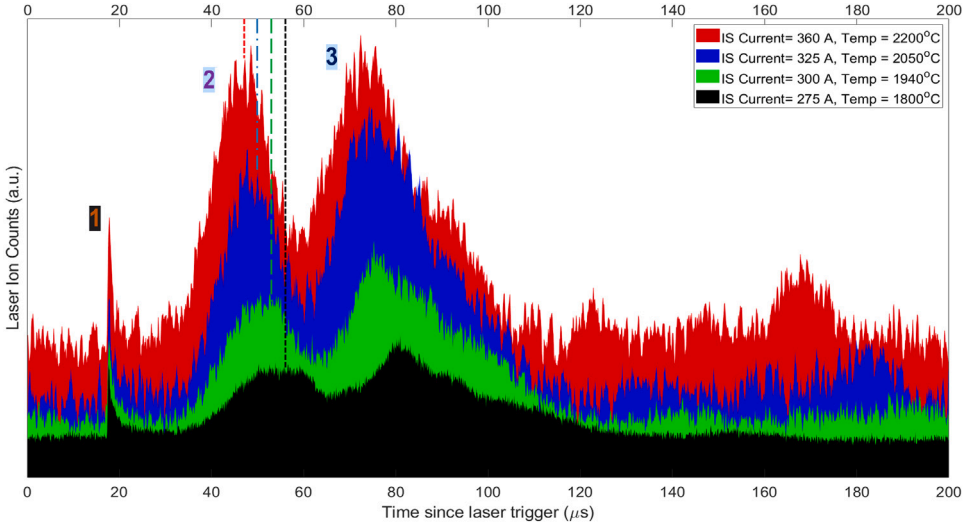


**Fig. 6.** Time structures of $^{71}$Ga laser ions at different ion source (IS) heating currents (temperatures). Temperatures 2200 °C, 2050 °C, 1940 °C, and 1800 °C indicated in red, blue, green, and black respectively. Dotted lines indicate the centroids of the second peaks at different temperatures.

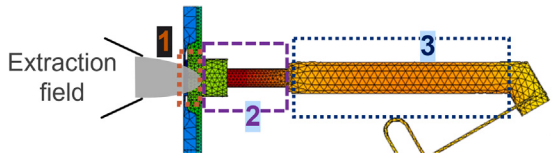


**Fig. 7.** Different sections of the ion source assembly in relation to the ion bunches produced. Region 1 indicates the outermost part of the ion source which is penetrated by the extraction field. Regions 2 and 3 indicate the hot cavity and the transfer line, respectively.

are shifted in time. Considering just the second peak for simplicity, the centroids of the peaks at different temperatures are indicated with the dotted lines of the corresponding color in Fig. 6. It is evident that the ions travel faster to the extraction zone (exit of the ion source) at higher temperatures. This effect can be explained simply by the higher voltage gradient at higher temperature, promoting a faster movement of the ions along the length of the ion source and transfer line volumes [12,29,30].

If the axial electric field is responsible for the movement of the ions inside the ion source, we should be able to track the origin of the second bunch in the time structure back to the hot cavity, taking into account the acceleration acting on the ions by the axial field. A FEM simulation of the axial electric field for different heating currents (temperature) is shown in Fig. 8. The axial electric field $E_x$ has an increasing trend at the very beginning of the transfer line (93–85 mm). It soon maintains a relatively constant value for the major part of the transfer line length (85–38 mm), until it exhibits a sudden drop where the transfer line is connected to the hot cavity (38–27 mm), due to sudden increase in the cross-section which decreases the electrical resistance by a large factor. In the majority of the hot cavity (27–5 mm), the axial field regains an almost constant value.

The electric field shows a slightly higher value in the transfer line compared to the hot cavity. This is due to the fact that the transfer line is thinner and has an effective cross-section of 10.6 $mm^2$ while the value in the hot cavity is 12.9 $mm^2$.

As it is known that the pre-bunch originates from the outermost part (close to the exit) of the ion source, this point can be used as a reference point for our calculations. The idea is to calculate the distance the ions would travel under the influence of the axial electric field during the time interval between the first pre-bunch and the peak of the second bunch.

The acceleration $a$ experienced by the ions with charge $q$ and mass $m$ in the axial electric field $E_x$ is given by

$$a = \frac{qE_x}{m} \tag{8}$$

Two main approximations are used for the calculations:

1. Initial ion velocities (thermal) are considered to be zero, as they have an isotropic distribution in all directions.
2. As the value of the axial field $E_x$ has a very low variance in the hot cavity at a given temperature, a mean value of $E_x$ is assigned for the hot cavity.

If $T_1$ is the temporal position of the pre-bunch and $T_2$ is the position of the second bunch in the time structure, $T_{21}$ indicates the time gap between them. Assuming zero initial velocity, the distance that the ions would have traveled during this time is given by,

$$L_{21} = \frac{1}{2}aT_{21}^2 \tag{9}$$

The deepest point inside the ion source that the extraction field of 30 kV can penetrate is 3.1 mm from the exit of the ion source. It corresponds to the pre-bunch at time $T_1$ and a value of $L_{10}$ = 3.1 mm can be assigned to this point.

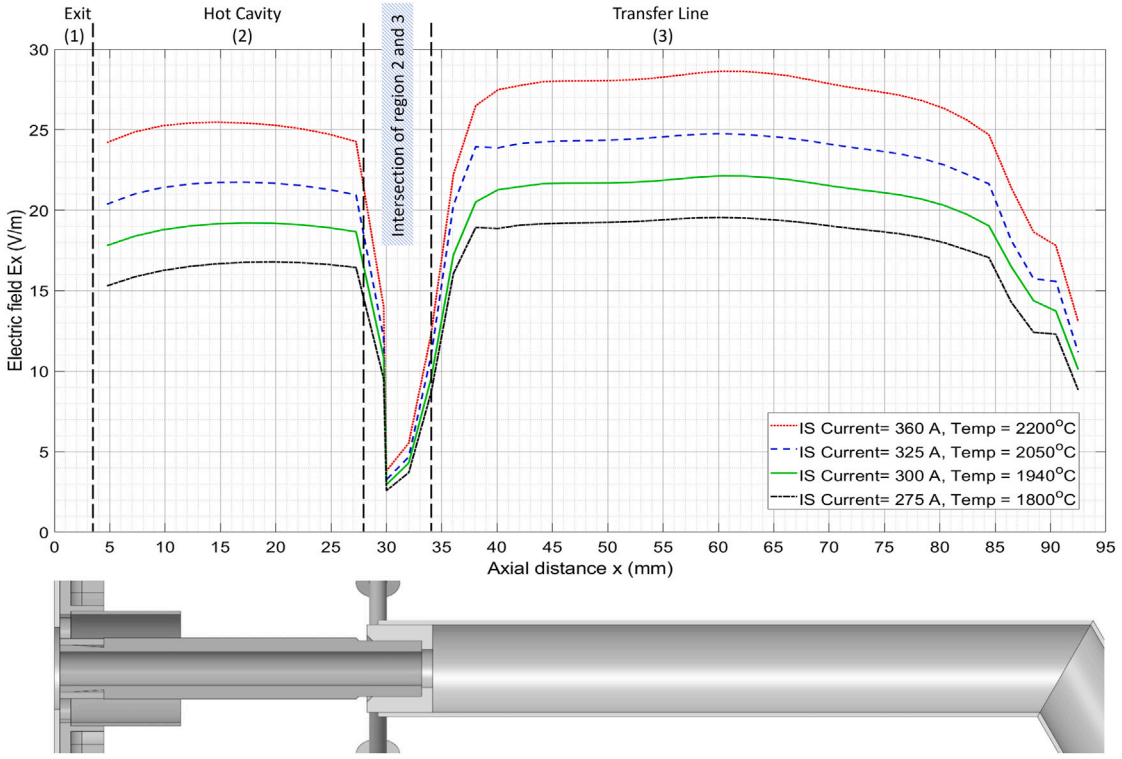


**Fig. 8.** FEM simulation of the axial electric field along the length of the ion source (IS) at different heating currents (temperatures). Temperatures 2200 °C, 2050 °C, 1940 °C and 1800 °C indicated in red, blue, green, and black respectively.

**Table 1**
Computation of the parameters related to the second bunch of ions in the time structure for different temperatures.

| Temp. (°C) | $T_1$ (μs) | $T_2$ (μs) | $T_{21}$ (μs) | Av. $E_x$ (V/m) | $L_{21\_calc}$ (mm) | $L_{10}$ (mm) | $L_{20}$ (mm) |
|---|---|---|---|---|---|---|---|
| 2200 | | 46.08 ± 0.15 | 28.24 ± 0.20 | 24.99 | 13.53 ± 0.19 | | 16.63 ± 0.19 |
| 2050 | 17.84 ± 0.05 | 47.72 ± 0.16 | 29.88 ± 0.21 | 21.34 | 12.93 ± 0.18 | 3.10 | 16.03 ± 0.18 |
| 1940 | | 49.23 ± 0.20 | 31.39 ± 0.25 | 18.82 | 12.59 ± 0.20 | | 15.69 ± 0.20 |
| 1800 | | 54.34 ± 0.53 | 36.50 ± 0.58 | 16.40 | 14.83 ± 0.47 | | 17.93 ± 0.47 |

To find the origin of the second bunch of ions relative to the exit of the ion source, the value $L_{20}$ can be simply evaluated as,

$$L_{20} = L_{21} + L_{10} \tag{10}$$

Table 1 shows the computed values of $L_{20}$ (on the rightmost column) for different ion source temperatures. All the values of $L_{20}$ are in agreement with the fact of the peak of the second bunch of ions originating from the mid-section of the hot cavity, whose total length is 33 mm. These values have been calculated by using the acceleration of the ions provided by just the axial electrical field, see Eq. (8). This shows that the axial field across the ion source plays a very critical role for the forces experienced by the ions drifting along the central axis of the source. This is in agreement with the work presented in [30].

Looking at Fig. 6, for the ion source at temperature 2050 °C (blue), a few smaller peaks start to appear after 100 μs (after the third main bunch). At 2200 °C (red), two small peaks appear around 122 μs and 147 μs, along with a much more prominent peak appearing at around 167 μs. These could be indications of slower ions formed deeper and at the very beginning of the transfer line. As seen from Fig. 8, the axial electric field at the beginning of the transfer line is lower compared to the rest of the transfer line. This lower axial field should essentially cause relatively slower movement of the ions originating here. As the design of this ion source has an angular bend at the beginning of the transfer line, it could possibly hint that the ions formed in this zone, undergo velocity change continuously to find the main axis of the ion source. Further detailed ion trajectory simulation investigations are foreseen in future work to complement this semi-quantitative approach presented here, also with special scope on ion confinement characteristics.

### 4.3. Laser enhancement ratio

Enhancement of the ion yield due to the laser effect was measured. For that, a Faraday Cup is inserted in front of the MagneTOF™ detector. The separation magnet was tuned to the gallium mass of 69 u for slightly better statistics as the natural abundance of $^{69}$Ga is higher compared to $^{71}$Ga. The lasers were set at a 10 kHz repetition rate, the working condition in the on-line production of isotopes. As the atoms or the species have an effusion time in the order of 100 μs, a repetition rate of 10 kHz provides a condition in which we expect that all atoms will encounter at least one laser pulse during their effusion through the hot cavity.

*Dependence on the power of the non-resonant step*

The cross-section of a non-resonant transition step is, generally, two to four orders of magnitude lower than that of a resonant transition. With the typically available pulse energy (1–4 mJ) used for such transitions, saturation is not expected to be reached and the ionization efficiency is directly proportional to the laser power available for the non-resonant excitation step.

At the ion source temperature of 2200 °C, the laser enhancement ratio was measured for various power of the green laser used for the non-resonant excitation, keeping the power of the UV fixed around 100 mW. The obtained values are plotted against the laser power, as shown in Fig. 9. The measurement indicates that the non-resonant step is saturated at only 1 mJ (10 W). This is inconsistent with the typically observed behavior at the ISOLDE RILIS where this ionization scheme is regularly used. In this case, we suspect that a power-dependent

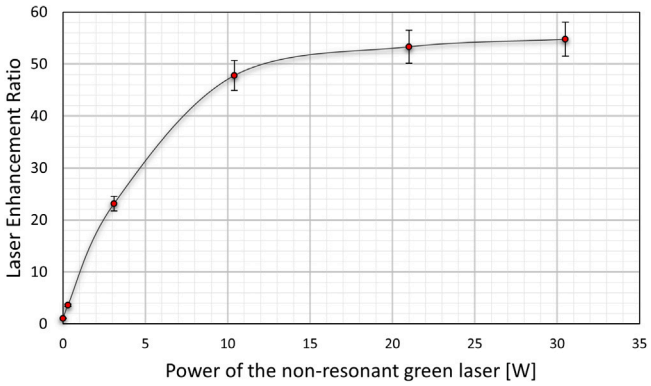


**Fig. 9.** Laser enhancement ratio at different power of the non-resonant green laser (532 nm) and fixed UV power of 100 mW, at ion source temperature of 2200 °C.

thermal lensing effect is occurring. Beyond 10 W, local heating of the vacuum entrance window is causing a defocussing of the green beam at the position of the ion source, resulting in a reduced power delivery efficiency.

Nevertheless, from this measurement, it could be safely inferred that we could operate the green laser with around 20 W of power without losing efficiency in the current setup.

*Dependence on the ion source temperature and the total ion current*

To understand the selectivity of the laser ion source at different ion source temperatures and different total ion currents (ion load), laser enhancement ratios (LERs) were measured for various combinations of the mentioned parameters, shown in Fig. 10. As indicated in Section 3.2, surface ionized barium was used to regulate the ion load in the ion source. The total extracted ion beam before mass separation serves as a measure for this quantity. During this measurement, the power of the UV and the green laser were maintained at 100 mW and 20 W, respectively.

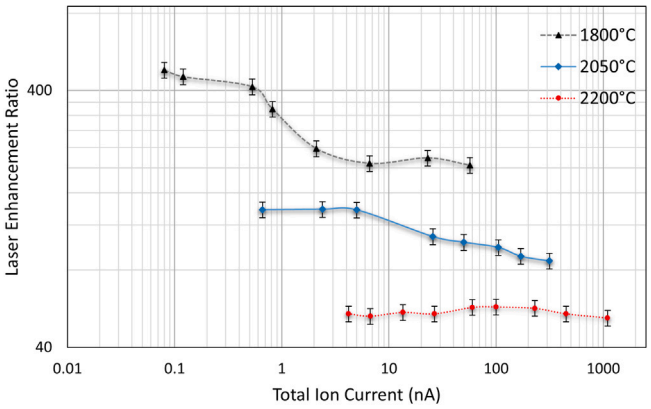


**Fig. 10.** Laser enhancement ratio (LER) at different ion source temperatures and total ion current. The ion source temperatures 1800 °C, 2050 °C and 2200 °C are indicated in black, blue, and red curves, respectively.

As can be seen from Fig. 10, the LER values remain nearly constant for the ion source temperature at 2200 °C. The values vary in the small range of 52.0–57.5 up to an ion load of 1.1 μA. At 2050 °C and 1800 °C, the LER values show dependency on the total ion current, hinting at an effective variation in the laser ion confinement at these temperatures. In the case of 2050 °C, the LER values decline from a starting value of 137 to a value of 87 while varying the total ion current from 660 pA to 315 nA. At 1800 °C, the LER value starts off with a high value of 480 at a total ion current of 80 pA and declines quickly until a value of 208 at an ion current of 7 nA and, remains more or less constant until a total ion current of 57 nA.

The relative surface ionization efficiency values at different temperatures for ionization of gallium ($W_i = 6$ eV) with tantalum ($\phi = 4.28$ eV) ion source could be calculated using Eqs. (3) and (4).

$$\beta_{2200} : \beta_{2050} : \beta_{1800} \simeq 1 : 0.6 : 0.2 \simeq 5 : 3 : 1 \tag{11}$$

The ratio provided above is for single atom-wall collision and serves to explain qualitatively the dropping LERs with increasing ion source temperatures. In practice, the amplification factor $N$ at different temperatures needs to be considered as well, since the effective ion survival factor also increases with rise in ion source temperature.

At the ion source temperatures of 1800 °C and 2050 °C, a declining trend in the value of LER is observed as the ion load is increased. This can be attributed to the temperature dependence of the thermionic electron density in the hot cavity (Eq. (7)). It follows therefore that, at higher temperatures the cavity ion capacity (the ion density at which the confining potential for ions is compromised), is greater.

At 2200 °C, the nominal working temperature of SPES ion source, and the maximum proton beam intensity (200 μA) on the $UC_x$ target, the total surface ion current is expected to be around 200 nA. From Fig. 10, it can be clearly confirmed that the selectivity of the laser ion source is not affected up to a total ion current of 1.1 μA, a value much higher than the expected maximum total ion current.

### 4.4. Ionization efficiency measurements

In this section, we report one measurement of surface ionization efficiency and three measurements of laser ionization efficiency, performed at an ion source temperature of 2200 °C and ion load conditions up to 110 nA of total beam, see Table 2.

*Surface ionization efficiency*

The surface ionization efficiency measurement was conducted with a sample size of 76 nAh and resulted in a value of 0.49% efficiency.

The theoretical surface ionization efficiency value for single atom-wall interaction can be calculated using Eqs. (2)–(4). At T = 2200 °C, the value of $\beta$ of gallium ($Q_i/Q_o = 0.22$, $W_i = 6$ eV) with tantalum ($\phi = 4.28$ eV) as ionizer material is calculated to be 0.007%. From the measurement, we find that the surface ionization efficiency value is $\beta_c = 0.49\%$, indicating an amplification factor of $N = 70.3$ (see Eq. (6)).

This measurement was done, also, to serve as a reference point to possibly co-relate the laser enhancement ratios and the laser ionization efficiency values.

*Laser ionization efficiency*

For the laser efficiency measurements, the laser powers used were: 100 mW (UV) and 20 W (green). The first two measurements were performed with sample sizes of 76 nAh and maintaining the isotope current of $^{69}$Ga around 4–5 nA. The third one was performed with a sample size of 114 nAh and an isotope current of around 7–8 nA. From the tests, it can be deduced that, under ideal conditions in terms of ion load, the SPES laser ion source can provide a laser efficiency of around 27.2% using the indicated gallium-scheme, laser powers, and 2200 °C ion source temperature.

A number of laser enhancement ratios (LERs) were also measured during all these efficiency tests by turning the laser on/off for just a few seconds (see Table A.3). The mean value of the LERs is around 55.5. It is quite evident that if the surface ionization efficiency value of 0.49% is multiplied by the obtained mean LER value of 55.5, we get a value of 27.2% which is very close to our obtained laser ionization efficiency value of 27.18%.

**Table 2**
Measured ionization efficiency values of gallium at ion source temperature 2200 °C.

| Test no. | Type | Efficiency (%) | Mean efficiency (%) |
|---|---|---|---|
| 1 | Surface | 0.49 ± 0.04 | 0.49 ± 0.04 |
| 2 | Laser | 27.66 ± 2.07 | |
| 3 | Laser | 27.64 ± 2.07 | 27.18 ± 1.18 |
| 4 | Laser | 26.23 ± 1.97 | |

It must be noted that, at 2200 °C, the ground state $3d^{10}4s^24p\ ^2P^\circ_{1/2}$ is only 45% populated assuming the Boltzmann distribution and the rest i.e. 55% population is in the state $3d^{10}4s^24p\ ^2P^\circ_{3/2}$ (826.19 cm$^{-1}$). In the gallium-scheme used in this experiment, a first step transition at 287.42 nm, between the zero level state $^2P^\circ_{1/2}$ and first excited state $4s^24d\ ^2D_{3/2}$, is used. If an additional laser at 294.36 nm is available, it is possible to make transitions to the neighboring excited state $^2D_{5/2}$ (34 787.85 cm$^{-1}$) from the state $^2P^\circ_{3/2}$. As the second step is a non-resonant step, the green laser will promote the electrons into the continuum regardless of whether it finds the electrons in $^2D_{3/2}$ or $^2D_{5/2}$ state after the first resonant excitation. In this case, the laser ionization efficiency could be almost doubled, according to [35].

## 5. Conclusions

The SPES laser ion source cavity has been characterized in terms of ion beam time structure, ion throughput for different operating temperatures, and ionization efficiency at 2200 °C for the ionization of gallium atoms. The surface ionization efficiency and time structure measurements indicates that the transfer line plays an important role in the overall laser and surface ion production. At the nominal operating temperature of 2200 °C, the cavity ion throughput (the ion rate at which no loss of laser ion performance is observed) exceeds 1 μA, an order of magnitude greater than has been measured for the standard ISOLDE RILIS cavity which has a passively heated transfer line without an axial extraction potential gradient. This could be attributed to the higher usable volume of the SPES ion source, as the transfer line is nearly as hot as the hot cavity and, also due to the presence of the axial potential gradient in the transfer line.

It is also observed that the ions are confined not only in the hot cavity but also in the transfer line, with a large fraction of the extracted ions originating inside the transfer line. It means that the confining plasma must also be present in the transfer line.

The axial electrical field has been demonstrated to provide the drifting acceleration of the ions along the length of the ion source. This aspect is important for the transport of the positive ions in the direction of the ion source extraction. These results are in accordance with the work presented in [30].

The laser enhancement ratios (LERs) are found to be almost independent of the total ion load at an ion source temperature of 2200 °C. This reflects a very stable laser ion confinement due to excess thermionic electrons created at this temperature, and hints to maintaining also constant laser ion source efficiency in this regime. At ion source temperatures of 2050 °C, the general behavior of LERs dropping with the increase in the ion load is observed. While in the case of 1800 °C, a sharp drop in the LERs is observed for a range of ion load and then, seem to stabilize after a certain value of ion load.

A laser ionization efficiency of 27.2% is reported for gallium using a resonant 287.42 nm (100 mW) and a non-resonant 532 nm (20 W). Use of an additional laser beam at 294.36 nm would allow us to potentially

further increase the ionization efficiency by 20%–30%, by accessing electrons in the thermally populated state $3d^{10}4s^24p\ ^2P^\circ_{3/2}$.

The SPES ion source has undergone several heating and cooling cycles during the calibration phase and during the measurement sessions, including power supply failures. The ion source continues to demonstrate very stable behavior, exhibiting a very high thermal robustness. The ion source is also now validated for use at SPES for high-power targets where the steady-state ion rate is expected to be 200 nA.

## CRediT authorship contribution statement

**O.S. Khwairakpam:** Conceptualization, Data curation, Formal analysis, Investigation, Methodology, Validation, Visualization, Writing – original draft, Writing – review & editing. **R. Mancheva:** Data curation, Investigation, Validation, Writing – review & editing. **M. Au:** Data curation, Software, Writing – review & editing. **C. Bernerd:** Data curation, Investigation. **L. Centofante:** Data curation, Investigation, Resources. **K. Chrysalidis:** Conceptualization, Methodology, Supervision, Writing – review & editing. **B. Crepieux:** Resources. **V.N. Fedosseev:** Conceptualization, Methodology, Resources, Validation, Writing – review & editing. **R. Heinke:** Conceptualization, Data curation, Investigation, Methodology, Validation, Writing – review & editing. **T. Marchi:** Funding acquisition, Project administration. **E. Mariotti:** Funding acquisition, Investigation, Supervision, Validation, Writing – review & editing. **B.A. Marsh:** Conceptualization, Methodology, Resources, Validation, Writing – review & editing. **A. Monetti:** Data curation, Resources. **P. Nicolosi:** Writing – review & editing. **S. Rothe:** Project administration. **D. Scarpa:** Conceptualization, Investigation, Methodology, Supervision, Writing – review & editing. **M. Schuett:** Data curation, Resources, Software. **T. Stora:** Project administration. **A. Andrighetto:** Project administration. **M. Manzolaro:** Funding acquisition, Project administration, Supervision, Validation, Writing – review & editing.

## Declaration of competing interest

The authors declare that they have no known competing financial interests or personal relationships that could have appeared to influence the work reported in this paper.

## Data availability

Data will be made available on request.

## Acknowledgments

This project has received funding from the European Union's Horizon 2020 research and innovation programme under grant agreement No 101008571 (PRISMAP – The European medical radionuclides programme).

It is also supported by funding from the Marie Sklodowska Curie Actions, ITN contract No. 861198 (LISA). We are grateful for the funding received from SPES (Italy), ISOLDE (Switzerland-France), and FWO-Vlaanderen (Belgium) to support this experiment. OSK has also used funds of the PhD course in Experimental Physics of the University of Siena.

We would like to dedicate this work to Dr. Bruce Marsh who passed away following a very unfortunate event in the end of 2023. He was a brilliant scientist and even more a wonderful person who always had a smile and good energy to share. He will be missed.

## Appendix. Laser enhancement ratios measured during the efficiency measurements

**Table A.3**
Measured laser enhancement ratios (LERs) during the efficiency measurements.

| No. | LERs | Mean LER |
|---|---|---|
| 1 | 56.1 | |
| 2 | 48.8 | |
| 3 | 54.8 | |
| 4 | 61.5 | |
| 5 | 57.5 | |
| 6 | 55.2 | |
| 7 | 60.5 | 55.5 (4.5) |
| 8 | 52.8 | |
| 9 | 57.5 | |
| 10 | 51.2 | |
| 11 | 47.7 | |
| 12 | 60.2 | |
| 13 | 61.4 | |
| 14 | 54.2 | |

## References

[1] O. Kofoed-Hansen, K.O. Nielsen, Short-lived krypton isotopes and their daughter substances, Phys. Rev. 82 (1) (1951) 96–97.
[2] Y. Blumenfeld, T. Nilsson, P. Van Duppen, Facilities and methods for radioactive ion beam production, Phys. Scr. T152 (2013) 014023.
[3] G. Prete, A. Andrighetto, J. Esposito, P. Mastinu, J. Wyss, The SPES project: a second generation ISOL facility, Phys. Procedia 26 (2012) 274–283.
[4] D. Scarpa, E. Mariotti, O.S. Khwairakpam, V. Parenti, A. Buono, P. Nicolosi, M. Calderolla, A. Khanbekyan, M. Ballan, L. Centofante, S. Corradetti, G. Lilli, M. Manzolaro, A. Monetti, L. Morselli, A. Andrighetto, New solid state laser system for SPES: Selective production of exotic species project at laboratori nazionali di legnaro, Rev. Sci. Instrum. 93 (8) (2022) 083001.
[5] A. Monetti, A. Andrighetto, C. Petrovich, M. Manzolaro, S. Corradetti, D. Scarpa, F. Rossetto, F. Martinez Dominguez, J. Vasquez, M. Rossignoli, M. Calderolla, R. Silingardi, A. Mozzi, F. Borgna, G. Vivian, E. Boratto, M. Ballan, G. Prete, G. Meneghetti, The RIB production target for the SPES project, Eur. Phys. J. A 51 (10) (2015).
[6] R. Kirchner, Ion sources for radioactive beams and related problems (Review) (invited), Rev. Sci. Instrum. 67 (3) (1996) 928–933.
[7] V. Fedosseev, K. Chrysalidis, T.D. Goodacre, B. Marsh, S. Rothe, C. Seiffert, K. Wendt, Ion beam production and study of radioactive isotopes with the laser ion source at ISOLDE, J. Phys. G: Nucl. Part. Phys. 44 (8) (2017) 084006.
[8] J. Lassen, R. Li, S. Raeder, X. Zhao, T. Dekker, H. Heggen, P. Kunz, C.D.P. Levy, M. Mostamand, A. Teigelhöfer, F. Ames, Current developments with TRIUMF's titanium-sapphire laser based resonance ionization laser ion source, Hyperfine Interact. 238 (1) (2017).
[9] V.S. Letokhov, Laser Photoionization Spectroscopy, Academic Press, San Diego, CA, 1987.
[10] G.S. Hurst, M.G. Payne, Principles and Applications of Resonance Ionisation Spectroscopy, Adam Hilger, Bristol, 1988.
[11] G.D. Alkhazov, V.S. Letokhov, V.I. Mishin, P.V. N, V.I. Romanov, S.K. Sekatsky, V.N. Fedoseyev, Highly effective Z-selective photoionization of atoms in a hot metallic cavity followed by electrostatic confinement of the ions, Pis'ma Zh. Techn. Fiz. 15 (63) (1989) 6.
[12] V. Mishin, V. Fedoseyev, H.-J. Kluge, V. Letokhov, H. Ravn, F. Scheerer, Y. Shirakabe, S. Sundell, O. Tengblad, Chemically selective laser ion-source for the CERN-ISOLDE on-line mass separator facility, Nucl. Instrum. Methods Phys. Res. B 73 (4) (1993) 550–560.
[13] G. Alkhazov, L. Batist, A. Bykov, V. Vitman, V. Letokhov, V. Mishin, V. Panteleyev, S. Sekatsky, V. Fedoseyev, Application of a high efficiency selective laser ion source at the IRIS facility, Nucl. Instrum. Methods Phys. Res. A 306 (1–2) (1991) 400–402.
[14] E.J. Prime, J. Lassen, T. Achtzehn, D. Albers, P. Bricault, T. Cocolios, M. Dombsky, F. Labrecque, J.P. Lavoie, M.R. Pearson, T. Stubbe, N. Lecesne, C. Geppert, K.D.A. Wendt, TRIUMF resonant ionization laser ion source, Hyperfine Interact. 171 (1–3) (2006) 127–134.
[15] Y. Liu, C. Jost, A.M. II, D. Stracener, C. Williams, C. Gross, R. Grzywacz, M. Madurga, K. Miernik, D. Miller, S. Padgett, S. Paulauskas, K. Rykaczewski, M. Wolinska-Cichocka, On-line commissioning of the HRIBF resonant ionization laser ion source, Nucl. Instrum. Methods Phys. Res. B 298 (2013) 5–12.
[16] M. Huyse, Ionization in a hot cavity, Nucl. Instrum. Methods Phys. Res. 215 (1–2) (1983) 1–5.
[17] R. Kirchner, On the thermoionization in hot cavities, Nucl. Instrum. Methods Phys. Res. A 292 (2) (1990) 203–208.

[18] J. Al-Khalili, E. Roeckl (Eds.), The Euroschool Lectures on Physics with Exotic Beams, 2006th ed., in: Lecture Notes in Physics, Vol. II, Springer, Berlin, Germany, 2006.
[19] É.Y. Zandberg, N.I. Ionov, Surface ionization, Sov. Phys. Uspekhi 2 (2) (1959) 255–281.
[20] T.K. Sato, M. Asai, A. Borschevsky, T. Stora, N. Sato, Y. Kaneya, K. Tsukada, C.E. Düllmann, K. Eberhardt, E. Eliav, S. Ichikawa, U. Kaldor, J.V. Kratz, S. Miyashita, Y. Nagame, K. Ooe, A. Osa, D. Renisch, J. Runke, M. Schädel, P. Thörle-Pospiech, A. Toyoshima, N. Trautmann, Measurement of the first ionization potential of lawrencium, element 103, Nature 520 (7546) (2015) 209–211.
[21] F. Schwellnus, R. Catherall, B. Crepieux, V.N. Fedosseev, B.A. Marsh, C. Mattolat, M. Menna, F.K. Österdahl, S. Raeder, T. Stora, K. Wendt, Study of low work function materials for hot cavity resonance ionization laser ion sources, Nucl. Instrum. Methods Phys. Res. B 267 (10) (2009) 1856–1861.
[22] H. Kawano, T. Takahashi, Y. Tagashira, H. Mine, M. Moriyama, Work function of refractory metals and its dependence upon working conditions, Appl. Surf. Sci. 146 (1–4) (1999) 105–108.
[23] M. Manzolaro, F. D'Agostini, A. Monetti, A. Andrighetto, The SPES surface ionization source, Rev. Sci. Instrum. 88 (9) (2017) 093302.
[24] F. Wenander, J. Lettry, M. Lindroos, Transverse emittance investigation of the ISOLDE target-ion sources, Nucl. Instrum. Methods Phys. Res. B 204 (2003) 261–266.
[25] S. Warren, T. Giles, C. Pequeno, A. Ringvall-Moberg, Offline 2, ISOLDE's target, laser and beams development facility, Nucl. Instrum. Methods Phys. Res. B 463 (2020) 115–118.
[26] M. Au, C. Bernerd, Y.N.V. Gracia, M. Athanasakis-Kaklamanakis, J. Ballof, M. Bissell, K. Chrysalidis, R. Heinke, L. Le, R. Mancheva, B. Marsh, J. Rolewska, M. Schuett, T. Venenciano, S. Wilkins, C. Düllmann, S. Rothe, Developments at CERN-ISOLDE's OFFLINE 2 mass separator facility for studies of molecular ion beams, Nucl. Instrum. Methods Phys. Res. B 541 (2023) 144–147.
[27] M. Schuett, M. Au, M. Bissell, N. Bidault, A. Koliatos, L. Le, N. Azaryan, R. Heinke, K. Chrysalidis, S. Rothe, Developments at the CERN-ISOLDE offline 2 mass separator, Nucl. Instrum. Methods Phys. Res. B 541 (2023) 82–85.
[28] D. Stresau, K. Hunter, W. Sheils, P. Raffin, Y. Benari, A new class of robust sub-nanosecond TOF detectors with high dynamic range, in: 54th ASMS Conference on Mass Spectroscopy, Seattle, Washington, 2006.
[29] J. Lettry, R. Catherall, G.J. Focker, O.C. Jonsson, E. Kugler, H. Ravn, C. Tamburella, V. Fedoseyev, V.I. Mishin, G. Huber, V. Sebastian, M. Koizumi, U.K. and, Recent developments of the ISOLDE laser ion source, Rev. Sci. Instrum. 69 (2) (1998) 761–763.
[30] Y. Liu, C. Baktash, J.R. Beene, C.C. Havener, H.F. Krause, D.R. Schultz, D.W. Stracener, C.R. Vane, C. Geppert, T. Kessler, K. Wies, K. Wendt, Time profiles of ions produced in a hot-cavity resonant ionization laser ion source, Nucl. Instrum. Methods Phys. Res. B 269 (23) (2011) 2771–2780.
[31] H.L. Ravn, S. Sundell, L. Westgaard, Target Techniques for the isolde on-line isotope separator, Nucl. Instrum. Methods 123 (1) (1975) 131–144.
[32] V. Fedosseev, L.-E. Berg, N. Lebas, O. Launila, M. Lindroos, R. Losito, B. Marsh, F. Österdahl, T. Pauchard, G. Tranströmer, J. Vannesjö, ISOLDE RILIS: New beams, new facilities, Nucl. Instrum. Methods Phys. Res. B 266 (19–20) (2008) 4378–4382.
[33] S. Rothe, B.A. Marsh, C. Mattolat, V.N. Fedosseev, K. Wendt, A complementary laser system for ISOLDE RILIS, J. Phys. Conf. Ser. 312 (5) (2011) 052020.
[34] V.N. Fedoseyev, G. Huber, U. Köster, J. Lettry, V.I. Mishin, H.L. Ravn, V. Sebastian, The ISOLDE laser ion source for exotic nuclei, Hyperfine Interact. 127 (2000) 409–416.
[35] B.A. Marsh, L.-E. Berg, D.V. Fedorov, V.N. Fedosseev, O.J. Launila, M. Lindroos, R. Losito, F.K. Österdahl, T. Pauchard, I.T. Pohjalainen, U. Sassenberg, M.D. Seliverstov, A.M. Sjödin, G. Tranströmer, The ISOLDE RILIS pump laser upgrade and the LARIS Laboratory, Hyperfine Interact. 196 (1–3) (2010) 129–141.